

**Solid-particle jet formation under shock-wave acceleration**V. Rodriguez,<sup>\*</sup> R. Saurel, G. Jourdan, and L. Houas<sup>†</sup>*Aix-Marseille Université, IUSTI, UMR CNRS 7343, Marseille, France*

(Received 21 January 2013; revised manuscript received 28 August 2013; published 12 December 2013)

When solid particles are impulsively dispersed by a shock wave, they develop a spatial distribution which takes the form of particle jets whose selection mechanism is still unidentified. The aim of the present experimental work is to study particle dispersal with fingering effects in an original quasi-two-dimensional experiment facility in order to accurately extract information. Shock and blast waves are generated in the carrier gas at the center of a granular medium ring initially confined inside a Hele-Shaw cell and impulsively accelerated. With the present experimental setup, the particle jet formation is clearly observed. From fast flow visualizations, we notice, in all instances, that the jets are initially generated inside the particle ring and thereafter expelled outward. This point has not been observed in three-dimensional experiments. We highlight that the number of jets is unsteady and decreases with time. For a fixed configuration, considering the very early times following the initial acceleration, the jet size selection is independent of the particle diameter. Moreover, the influence of the initial overpressure and the material density on the particle jet formation have been studied. It is shown that the wave number of particle jets increases with the overpressure and with the decrease of the material density. The normalized number of jets as a function of the initial ring acceleration shows a power law valid for all studied configurations involving various initial pressure ratios, particle sizes, and particle materials.

DOI: [10.1103/PhysRevE.88.063011](https://doi.org/10.1103/PhysRevE.88.063011)

PACS number(s): 47.40.Nm, 45.70.-n

**I. OBJECTIVES**

During the past decade, many investigations have been carried out to determine the physical mechanisms that govern particle jet formation during the dispersal of a granular medium exposed to an impulsive pressure load, i.e., shock and blast waves. This physical phenomenon is observed with spherical explosions, with charges surrounded by particles, or in nature, e.g., with volcanic eruptions [1]. The formation of particle jets is also observed during impact of solid projectile on granular media [2]. Most of previous experimental observations have been carried out so far in three-dimensional quasi-spherical configurations using explosives surrounded by granular layers [3–7]. The attempt was to correlate the particle jet sizes to initial parameters such as particle diameter and density, particle layer thickness, and strength of the incident shock load in order to understand the breaking mode of a solid particle cluster. But the 3D nature of this configuration has not helped to identify the origin of the jet selection. More recently, cylindrical experiments were performed by Frost *et al.* [8], where it was easier to visualize the particle jet spread. Even if it has been shown that the formation of particle jets depends both on the particle material properties and on the ratio between the particle layer mass and the explosive mass [3], the physical mechanism of the particle jet selection is still missing. In the present work we study particle dispersal with fingering effects in quasi-two-dimensional configurations using moderate pressure loads induced by shock-tube-type facilities connected to a Hele-Shaw cell. With this convenient experimental setup it is possible to conduct repetitive reliable experiments using a ring of particles in radial expansion trapped in a Hele-Shaw cell. The paper is organized as follows. In Sec. II, we detail the experimental setup and focus on

the experimental protocol. In Sec. III, we present the results, namely the experimental observations, the influence of the cell gap, the influence of the initial pressure load impulse, and density of particles on the jet formation. In Sec. IV, we summarize the results obtained in these experimental campaigns, in particular regarding reduced laws.

**II. EXPERIMENTAL SETUP**

The present experimental study is carried out using a quasi-two-dimensional facility in order to observe both inner and outer interfaces of the particle layer during particle dispersal. A  $1900 \times 1500 \times 4 \text{ mm}^3$  Hele-Shaw cell is used inside which a particle ring is set to motion by a pressure pulse directly initiated in the center of the particle ring as shown in Fig. 1. Generally, typical Hele-Shaw cell configurations present very small gaps ranging from 0.1 to 2 mm. For these characteristic gap sizes, three-dimensional effects can be neglected. In our case, the gap between the plates was larger (4 mm) to have a sufficient amount of granular matter. The gap influence is discussed subsequently and is shown to be negligible. This type of facility has already been used successfully for observation of granular fingering instabilities [9]. In that case, finger patterns were obtained after the displacement of fine granular material by the gas flow. Existence of fractal structures was observed in those experiments. The present experiments consider much more dynamic flow situations, closed to configurations involving explosives. A small conventional vertical shock tube (T32) and a pressurized tank (T100) were alternatively vertically fitted beneath the Hele-Shaw cell. The first creates a blast wave at its exit, i.e., an impulsive pressure jump followed by a rapid pressure decrease. Its driver section is 210 mm long and its driven section is 945 mm long with a diameter of 32 mm. Most of the experiments were carried out with this tube. The second tank produces a sustained shock wave, i.e., an impulsive pressure jump followed by a constant plateau. The pressurized

<sup>\*</sup>vincent.rodriquez@etu.univ-amu.fr<sup>†</sup>lazhar.houas@univ-amu.fr

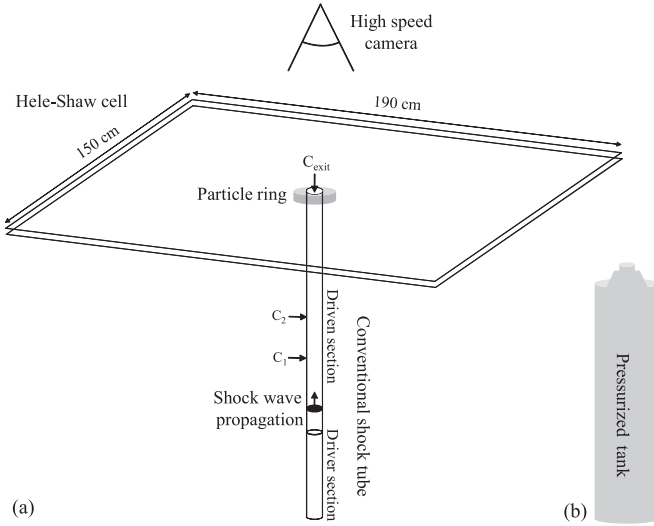


FIG. 1. Sketch of the experimental setup composed of a 4-mm-width Hele-Shaw cell and (a) a conventional shock tube or (b) a pressurized tank vertically fitted beneath the cell.

tank is 1150 mm long and 100 mm in diameter with a reduction of 32 mm at the exit section. The aim of this gas tank is to modify the pressure load profile exerted to the particle ring and to study the influence of this one on the jet formation.

We have chosen to use moderate overpressures in order to better observe details during the particle dispersal. The granular material consisted of a ring of flour or polystyrene particles disposed in the center of the cell and gently loaded between the plates using a mold around the outlet of the pressure generator and confined in a two-dimensional geometry allowing radial dispersion only. Three pressure piezosensitive gauges were mounted on the present experimental setup. Two of them ( $C_1$  and  $C_2$ ) were located along the conventional shock tube T32 in order to determine the incident shock wave Mach number. The third ( $C_{\text{exit}}$ ) recorded the pressure history at the center of the particle ring. To record the evolving flow pattern in the cell, a high-speed digital camera Photron Fastcam SA1 was used with an acquisition frequency of 4000 fps and a spacial resolution of  $1024 \times 1024$  pixels.

### III. RESULTS

#### A. Experimental observations

In Fig. 2, an example of the breaking process of a solid particle ring confined in a radial two-dimensional geometry, issued from the experimental device, is presented. As flour particles are cohesive, it is difficult to measure the real mean diameter of a single particle. The most referenced mean value for the used flour (the thinnest flour) is  $10 \mu\text{m}$  [10,11]. The initial experimental conditions are grouped in Table I.

The present experimental observations highlight the presence of various perturbations in granular media when exposed to a pressure pulse, in addition to the particle jets already observed in three-dimensional configurations. Moreover, the two-dimensional configuration allows observation inside the particle ring during its dispersion, which never has been done before.

At  $t = 0$  the blast wave issued from the discharge of a planar shock wave from the open exit shock tube interacts with the particle ring [Fig. 2(a)] and the dispersion starts. First, following the initial pressure load, the particle ring moves radially, showing a perfect smooth external interface. However, not all particles around the inner ring surface have the same velocity. Some particles are slower than others resulting in particle concentration fluctuation as shown in Fig. 2(b). Particle jets appear regularly around the inner surface of the ring. These internal particle jets are denoted  $J_i$  in the following. Then, short-wavelength perturbations appear on the outer surface of the ring as shown in Fig. 2(c). The wavelength of these small perturbations (along the ring outer surface) is smaller than that observed for the internal jets  $J_i$ . It appears that this wavelength is independent of the incident shock wave (or pressure load impulse). These very thin external jets at short time, denoted by  $J_e^{\text{st}}$  tend to disappear at long times. Afterwards, the particle front velocity decreases while the internal particle jets  $J_i$  continue to move in the same direction with the same velocity. Consequently, they cross the front and are expelled outside, as shown in Fig. 2(a) at  $t = 20$  ms. Finally, these larger external jets at long times, denoted by  $J_e^{\text{lt}}$ , start their growth [Fig. 2(a) from  $t = 20$  ms to  $t = 60$  ms]. At very long times ( $t = 100$  ms) the number of external jets, noted  $J_e^{\text{vlt}}$ , decreases with time (this point will be described in more detail later). To summarize, there are four characteristic steps. At early times internal jets  $J_i$  appear around the inner surface of the ring. Then very thin external jets  $J_e^{\text{st}}$  appear all around the outer surface of the ring. At long times, the external jets  $J_e^{\text{lt}}$  emanating from the internal jets  $J_i$  appear. Last, at very long times, the external jets  $J_e^{\text{vlt}}$ , resulting of previous  $J_e^{\text{lt}}$  jets, coalesce because of the transverse motion induced by friction effects.

Figure 2(d) presents a superposition of two frames taken at  $t = 6$  ms and  $t = 57$  ms, respectively, clearly showing the coincidence between  $J_i$  and  $J_e^{\text{lt}}$  structures. These two frames were extracted from the experiments shown in Fig. 2(a). Indeed, it is apparent that  $J_i$  and  $J_e^{\text{lt}}$  jets are aligned, in the present case, with the same number of particle jets.

Furthermore, from the recorded pictures, the trajectories of both the particle front and the particle jets versus time have been reconstructed as shown in Fig. 3 and analyzed. The crossing trajectories confirm that the jets grow inside the particle ring before crossing the front at about 13 ms for this experiment.

As mentioned above, the number of external jets decreases with time. It is important to note that the process of the jet selection is unsteady, i.e., the number of the jets  $N_j$  evolves with time, as illustrated in Fig. 4. From this figure, it is clear that the number of jets is constant from  $t = 0$  to  $t = 45$  ms and then decreases with time, possibly induced by friction effects [12].

#### B. Influence of the cell gap on the jet formation

The gap influence in the Hele-Shaw cell has been investigated by varying its amplitude from 1 to 10 mm in order to choose the best width. The experimental conditions are presented in Table II. Whatever the Hele-Shaw cell gap was, the developed flow patterns induced by the radial expansion of the granular medium was the same ( $J_i$ ,  $J_e^{\text{st}}$ , and  $J_e^{\text{lt}}$ ).

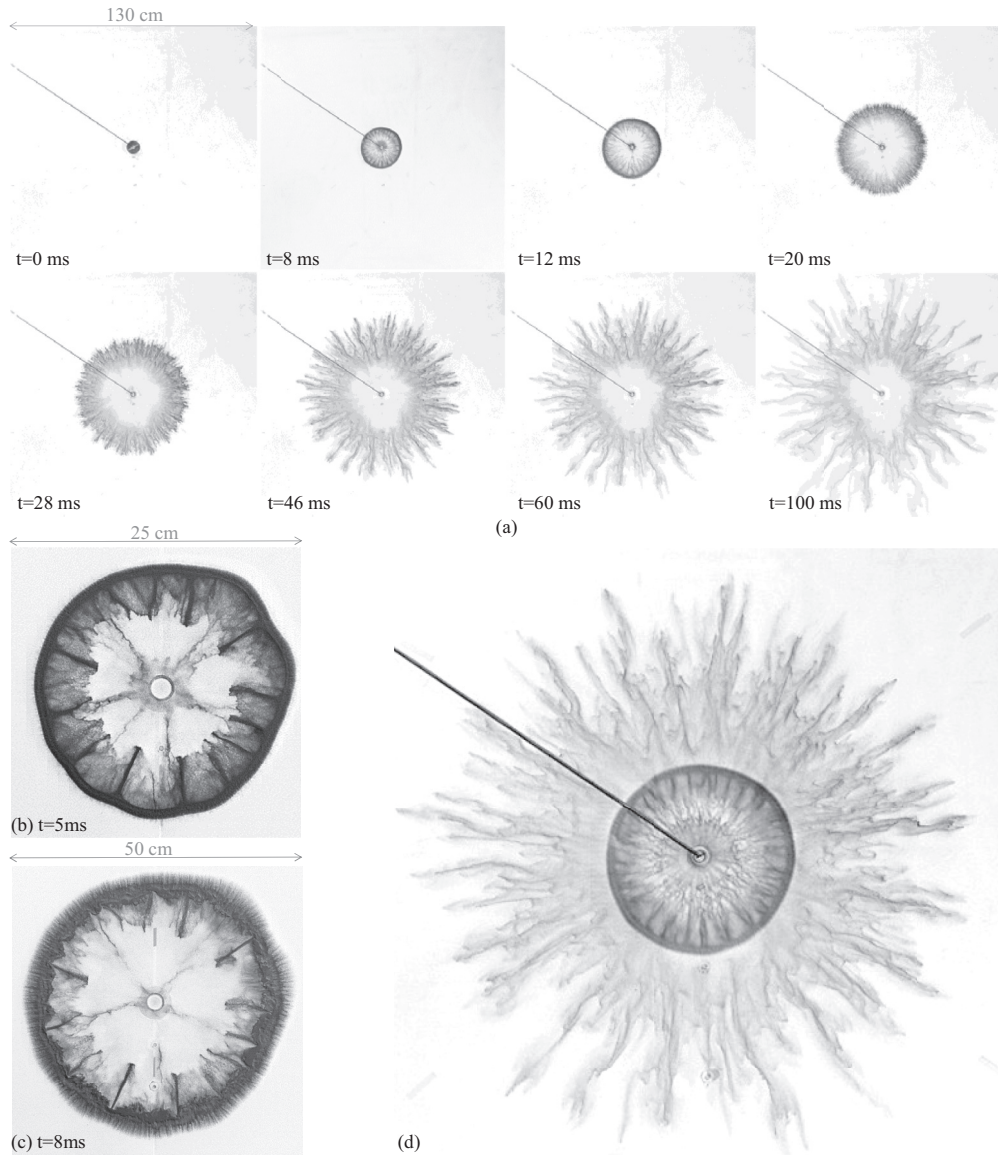


FIG. 2. (a) Sequence of recorded photographs covering jet formation of flour particles set to motion by a 1.16 Mach number shock wave. (b) Magnified view of internal jets extracted at 5 ms after the initial acceleration. (c) Magnified view of external front perturbations extracted at 8 ms after the initial acceleration. (d) Superposition of two frames taken at 6 and 57 ms after the initial acceleration showing the correlation between internal and external particle jets (not to scale). On the top left, the connexion wire of the pressure sensor  $C_{exit}$ .

Consequently, in the range of the gap widths considered, no significant perturbation variation appeared. However, on one hand, we have to impose a minimum width to have enough particles into the cell to observe the entire jet formation. On the other hand, if the gap is excessive, the visualization of the particle motion into the cell can be perturbed with the

TABLE I. Initial experimental conditions where  $\rho_p$ ,  $\Phi_p$ ,  $D_{ext}$ ,  $e$ ,  $M_{sw}$ , and  $\Delta P_{C_{exit}}$  are the material density (in  $kg/m^3$ ), the particle diameter (in  $\mu m$ ), the ring external diameter (in mm), the particle layer thickness (in mm), the incident shock wave Mach number, and the initial overpressure load peak (in bars), respectively.

Particles	$\rho_p$	$\Phi_p$	$D_{ext}$	$e$	$M_{sw}$	$\Delta P_{C_{exit}}$	Generator
Flour	1530	10	60	20	1.16	1.3	T32

superposition of several layers. Based on this preliminary experimental study, we chose to set a 4-mm gap between the plates, where a reasonably two-dimensional evolution is observed. We also checked that the space between the plates remained constant during the experiments. Some thin wedges were inserted between the plates and near the center to prevent the top plate to bend under its weight. Then, to be sure that the gap stayed constant under shock loading, we visualized the motion of the top plate. The maximum amplitude of the deformation was less than 10% (about 0.4 mm) of the gap width for the first oscillation and then relaxed very quickly.

**C. Influence of the pressure pulse profile**

In order to better identify the origin of the formation and selection of the jets, we consider other experiments

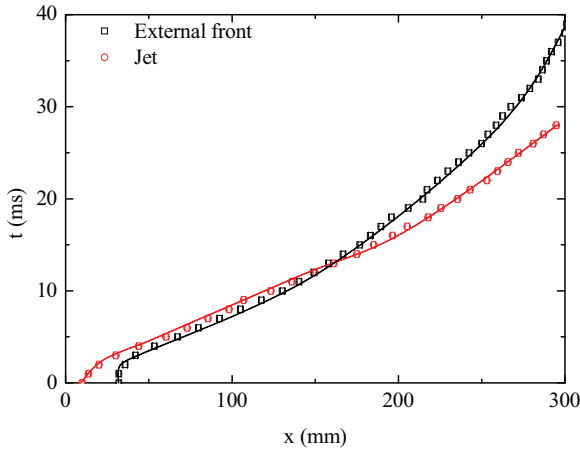


FIG. 3. (Color online)  $x-t$  diagram showing the position of the external particle front and the jet head relative to the center of the particle ring, exposed to a 1.16 Mach number shock wave, for the T32 impulse load. The particle material is flour.

with different pressure stimuli. Indeed, with the shock tube facility, the pressure pulse in the particle cloud corresponds to a blast wave and various waves reflections occur inside the tube, resulting in oscillations. In order to remove these oscillations and consider a simpler pressure signal, the shock tube is replaced by a tank that is 100 mm in diameter. The corresponding volume is 50 times larger than that of the T32 shock tube. It is made of a driver section only, directly fitted beneath the Hele-Shaw cell. A schematic representation of the T100 tank is shown in Fig. 1(b). The modification of the experimental facility changes the overpressure profile versus time at the center of the particle ring and makes it constant after the pressure jump, as seen in the top part of Fig. 5. It shows a comparison between the different overpressure conditions to which the particle ring is submitted. Although these two pressure shapes clearly differ, we observe that the jet formation during the solid particle dispersal in both cases is very similar. Indeed, the presence of the various perturbations, i.e.,  $J_i$ ,  $J_e^{st}$ ,  $J_e^{lt}$ , are all observed quasi-identically. Moreover, the number of particle jets is similar in both cases. As we

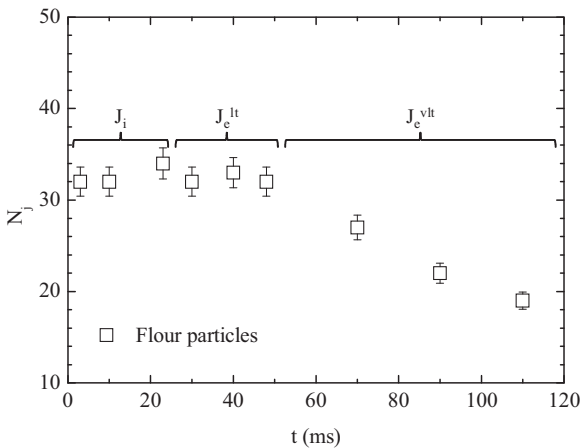


FIG. 4. Time evolution of the number of jets  $N_j$  ( $J_i$ ,  $J_e^{lt}$ , and  $J_e^{vlt}$ ) obtained in the case of a ring of flour accelerated by an incident 1.16 Mach number shock wave.

TABLE II. Initial experimental conditions where  $\rho_p$ ,  $\Phi_p$ ,  $D_{ext}$ ,  $e$ ,  $M_{sw}$ , and  $\Delta P_{C_{exit}}$  are the material density (in  $\text{kg/m}^3$ ), the particle diameter (in  $\mu\text{m}$ ), the ring external diameter (in mm), the particle layer thickness (in mm), the incident shock wave Mach number, and the initial overpressure load peak (in bars), respectively.

Particles	$\rho_p$	$\Phi_p$	$D_{ext}$	$e$	$M_{sw}$	$\Delta P_{C_{exit}}$	Generator
Flour	1530	10	60	20	1.40	3.5	T32

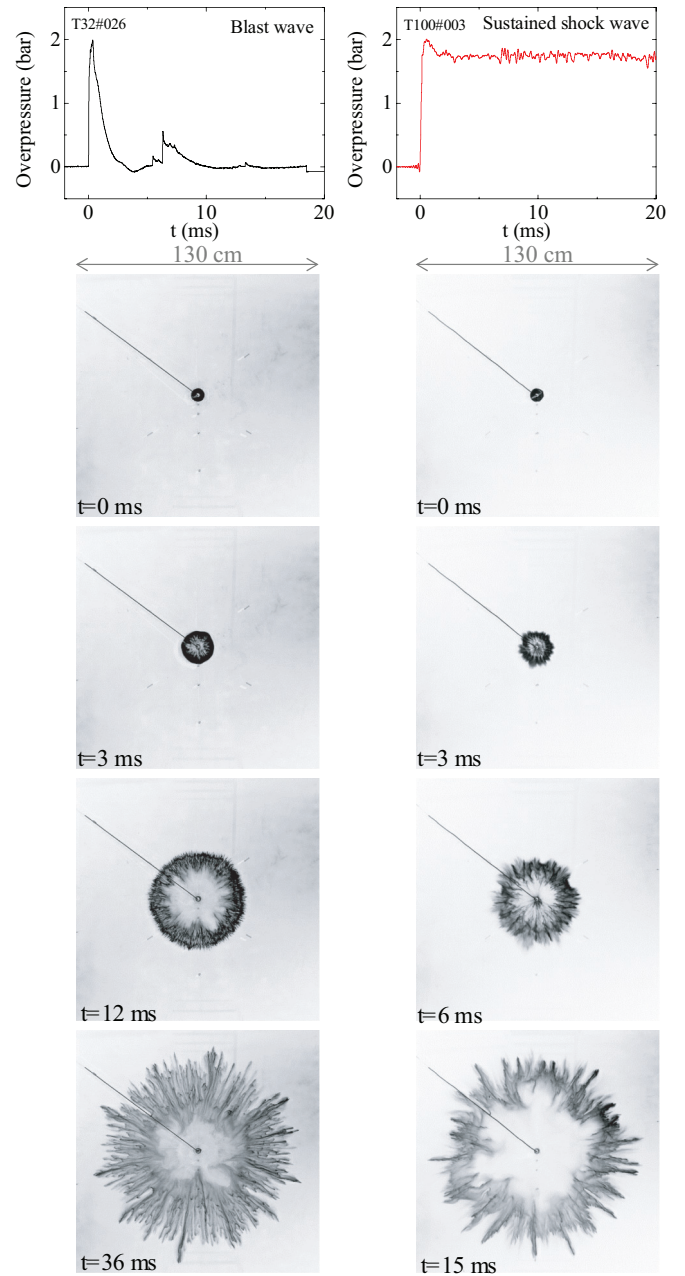


FIG. 5. (Color online) Comparison between particle jet development obtained for two different pressure pulses. The left column shows the evolution of a flour particle ring submitted to a blast wave (T32). The right column shows the evolution of the same particle ring submitted to a sustained shock wave (T100). In both cases, the initial overpressure peaks measured in the center of the rings were 2 bars. Similar phenomenon are observed in both cases.

TABLE III. Initial experimental conditions where  $\rho_p$ ,  $\Phi_p$ ,  $D_{\text{ext}}$ ,  $e$ ,  $M_{\text{sw}}$ , and  $\Delta P_{C_{\text{exit}}}$  are the material density (in  $\text{kg}/\text{m}^3$ ), the particle diameter (in  $\mu\text{m}$ ), the ring external diameter (in mm), the particle layer thickness (in mm), the incident shock wave Mach number, and the initial overpressure load peak (in bars), respectively.

Particles	$\rho_p$	$\Phi_p$	$D_{\text{ext}}$	$e$	$M_{\text{sw}}$	$\Delta P_{C_{\text{exit}}}$	Generator
Polystyrene	1050	10–250	60	20	1.37	2	T32

can see in Fig. 5 on pictures taken from  $t = 0$  to  $t = 3$  ms, the particle expansion velocity seems to be quite the same. But later, as time goes on, particle jets develop faster for the shock wave configuration (T100) than for the blast wave (T32) one. Note that the duration of the pressure positive phase is about 3 ms for the T32 excitation and more than 20 ms for the T100 case. Consequently, the expansion velocity of the particle ring decreases for the T32 case but remains constant for the T100 case. In addition, the jet selection is already achieved before 2 ms ( $J_i$  are visible). Consequently, even if the particles in the T32 experiments continue moving with their inertia after 3 ms while particles in the T100 experiments continue their acceleration, the number of particle jets is early fixed to  $24 \pm 1$  jets in both experiments. We can conclude that the particle jet selection is not correlated to the shape of the pressure pulse and, in particular, to the presence of pressure oscillations.

#### D. Influence of the particle diameter

Experiments have been carried out for polystyrene spheres with different diameters ranging from 10 to 250  $\mu\text{m}$ . This was done with the experimental conditions summarized in Table III. Figure 6 shows the evolution of the number of particle jets  $N_j$ , determined at early times, as a function of the particle diameter  $\Phi_p$ . It shows that the early time number of particle jets is independent of the particle diameter, in agreement with the previous observations done with liquids and powders [12].

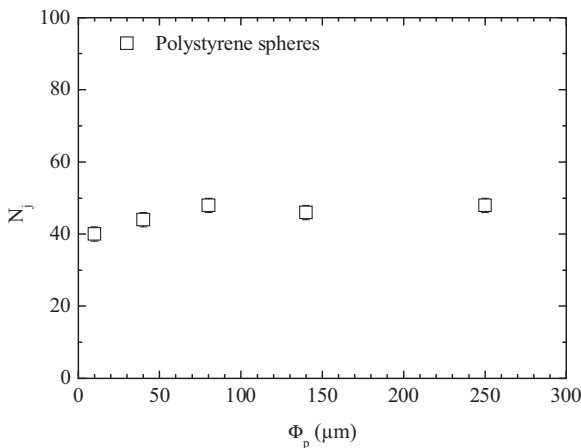


FIG. 6. Number of particle jets  $N_j$  at early times ( $J_i$ ) versus the particle diameter  $\Phi_p$  determined in the case of an incident shock wave of 1.37 Mach number ( $\Delta P_{C_{\text{exit}}} = 2\text{bars} \pm 0.4$  bar).

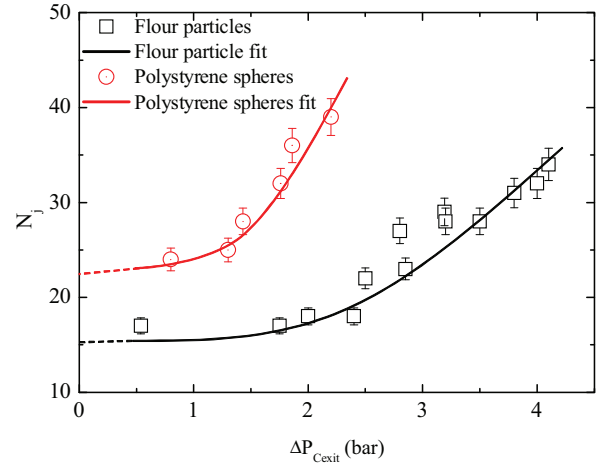


FIG. 7. (Color online) Number of particle jets  $N_j$  ( $J_i$  or  $J_e^{\text{lt}}$ ) versus the initial overpressure peak in the center of the particle ring  $\Delta P_{C_{\text{exit}}}$  obtained for flour and polystyrene spheres of 10  $\mu\text{m}$  in diameter. The density of flour particles and polystyrene spheres are 1530 and 1050  $\text{kg}/\text{m}^3$ , respectively.

#### E. Influence of the initial pressure impulse and density of particles

A series of experiments conducted with the T32 blast-wave generator has been carried out for different initial overpressure peaks (ranging from 0.5 to 4.1 bars) and two different particle materials (flour particle and polystyrene spheres with a material density of 1530 and 1050  $\text{kg}/\text{m}^3$ , respectively, and particle diameter of 10  $\mu\text{m}$ ). The same particle ring dimensions (external and internal diameter of 60 and 20 mm, respectively) were set.

We have plotted in Fig. 7 the number of particle jets  $N_j$  (for  $J_i = J_e^{\text{lt}}$ ) as a function of the initial overpressure peak at the center of the particle ring  $\Delta P_{C_{\text{exit}}}$  for each configuration. This graph confirms that the number of particle jets, after the impulsive acceleration, increases with the initial pressure pulse amplitude. We can see that for both particle materials, the number of jets evolution presents the same asymptotic tendency for low-pressure loads. Moreover, Fig. 7 clearly points out the influence of the material density on the number of jets. For an identical initial overpressure pulse imposed to the ring of particles, the number of jets increases when the material density decreases. In order to merge all the experimental points on the same curve, we have represented in Fig. 8 the number of jets  $N_j$  versus the overpressure  $\Delta P_{C_{\text{exit}}}$  multiplied and divided respectively by the ratio of material densities  $R$ :  $R = \rho_{\text{flour}}/\rho_{\text{polystyrene}}$ . It puts in evidence that the number of jets is inversely proportional to the material density. Fit curves have been obtained using the following relationships, based on the work of Ripley *et al.* for dry powders:  $N_j = C P^k$ , where  $C$  and  $k$  are constant parameters and  $P$  is the flow pressure. We have slightly modified this relation in order to better fit the present experimental results as  $N_j = C_0 + C \Delta P_{C_{\text{exit}}}^k$ , where  $C_0$ ,  $C$ , and  $k$  are constant parameters and  $\Delta P_{C_{\text{exit}}}$  is the initial overpressure peak at the center of the particle ring. Based on the present experimental data, the correlation takes the following form:  $N_j R = 22 + 3.35(\Delta P_{C_{\text{exit}}}/R)^{2.1}$ . In addition,

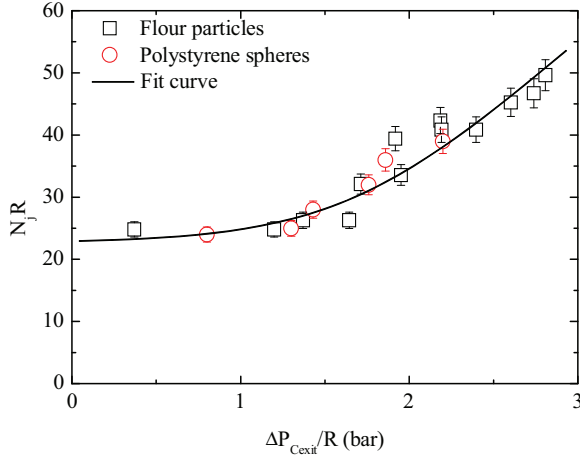


FIG. 8. (Color online) Number of particle jets  $N_j$  ( $J_i$  or  $J_e^{lt}$ ) multiplied by the ratio of material densities  $R$  versus the initial overpressure peak  $\Delta P_{C_{exit}}$  divided by  $R$ . The fit curve equation is  $N_j R = 22 + 3.35(\Delta P_{C_{exit}}/R)^{2.1}$ .

it shows that the number of particle jets is dependent to the particle layer acceleration. Until now, experiments were conducted for a particle layer thickness of 20 mm and an external ring diameter of 60 mm. Another experiment has been carried out for an identical particle layer thickness but an external ring diameter of 90 mm. Thus, in order to be able to compare all these experiments in a same graph, we have normalized the  $(N_j R)$  axis by the initial ring perimeter  $p_{er}$ . Consequently, the  $N_j R$  variable is expressed per unit length. Figure 9 represents  $(N_j R)/p_{er}$  as a function of the particle layer acceleration, deduced from the experimental reconstructed trajectories, between 0 and 3.5 ms, fitted by following equation:  $(N_j R)/p_{er} = 128.5 + 0.14\gamma^{2.6}$ , where  $\gamma$  represents the particle cloud acceleration. As we can see, the experimental points for both flour and polystyrene spheres and for both 60 and 90 mm external diameter are merged, as shown in Fig. 9. Then we can conclude that the number of particle jets ( $J_i$  and  $J_e^{lt}$ ) is directly linked to the external perimeter and to the initial acceleration of the particle layer.

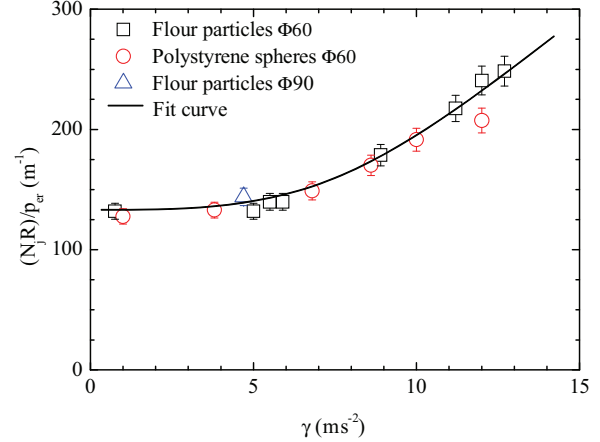


FIG. 9. (Color online)  $(N_j R)/p_{er}$  versus the particle layer acceleration between 0 to 3.5 ms. The fit curve equation is  $(N_j R)/p_{er} = 128.5 + 0.14\gamma^{2.6}$ .

#### IV. CONCLUSION

An experimental study of particle jet formation associated to the motion of a granular material subjected to blast or shock waves has been conducted in a Hele-Shaw cell. The effects of particle diameter, pressure load, particle density, and ring size have been studied. From high-speed visualizations, we observe that particle jets form first inside the particle ring before being expelled outside. It also appears that the jet selection mechanism which takes place at very early times ( $J_i$ ) seems to be independent of both the pressure pulse shape and the particle diameter. It is pointed out that the number of jets increases with the pressure load, and consequently with the initial acceleration, following a power law of the form  $N_j R = C_0 + C(\Delta P_{C_{exit}}/R)^k$ . In addition, it is shown that the jet number decreases with the increase of the material density and remains proportional to the ring external perimeter following a power law of the form  $(N_j R)/p_{er} = 128.5 + 0.14\gamma^{2.6}$ .

#### ACKNOWLEDGMENTS

Part of this work was supported by CEA Gramat. E. Lapébie is gratefully acknowledged.

- 
- [1] V. Kedrinsky, *Shock Waves* **18**, 451 (2009).  
 [2] D. Lohse, R. Bergmann, R. Mikkelsen, C. Zeilstra, D. van der Meer, M. Versluis, K. van der Weele, M. van der Hoef, and H. Kuipers, *Phys. Rev. Lett.* **93**, 198003 (2004).  
 [3] D. L. Frost, S. Goroshin, and F. Zhang, in *Proceedings of the 21st Military Aspects of Blast and Shock, CD-Rom* (ORTA, Jerusalem, Israel, 2010), p. 36; [http://www.mabs.ch/spiezbase/mabs21/Abstracts%20CORRECT%20with%20Page%20No\\_S35.pdf](http://www.mabs.ch/spiezbase/mabs21/Abstracts%20CORRECT%20with%20Page%20No_S35.pdf).  
 [4] F. Zhang, D. L. Frost, P. A. Thibault, and S. B. Murray, *Shock Waves* **10**, 431 (2001).  
 [5] D. L. Frost, C. Ornthalalai, Z. Zarei, V. Tanguay, and F. Zhang, *J. Appl. Phys.* **101**, 113529 (2007).  
 [6] A. M. Milne, C. Parrish, and I. Worland, *Shock Waves* **20**, 41 (2010).  
 [7] C. Parrish and I. Worland, in *Proceedings of the 28th International Symposium on Shock Waves*, edited by K. Kontis (Springer, Manchester, 2011), Vol. 2, p. 107.  
 [8] D. L. Frost, Y. Grégoire, P. Oren, S. Goroshin, and F. Zhang, *Phys. Fluids* **24**, 091109 (2012).  
 [9] X. Cheng, L. Xu, A. Patterson, H. M. Jaeger, and S. R. Nagel, *Nat. Phys.* **4**, 234 (2008).  
 [10] B. Sullivan, W. E. Engebretson, and Merlin L. Anderson, *Cereal Chemistry* **37**, 436 (1960).  
 [11] R. R. Irani and W. S. Fong, *Cereal Chemistry* **38**, 67 (1961).  
 [12] R. C. Ripley, L. Donahue, and F. Zhang, *AIP Conf. Proc.* **1426**, 1615 (2012).